



# Dimensionality effects in crystal plasticity, from 3D silicon to 2D silicene

Evgeniya Dontsova<sup>a,\*</sup>, Roberto Ballarini<sup>b</sup>, Boris I. Yakobson<sup>c</sup>

<sup>a</sup> Enovate Upstream, Spring, TX, 77386, USA

<sup>b</sup> Department of Civil and Environmental Engineering, University of Houston, Houston, TX 77204, USA

<sup>c</sup> Department of Materials Science and Nanoengineering, Department of Chemistry, and the Smalley Institute, Rice University, Houston, TX 77005, USA

## ARTICLE INFO

### Article history:

Received 9 May 2020

Received in revised form 12 July 2020

Accepted 16 July 2020

Available online 22 July 2020

## ABSTRACT

To characterize the effects of free surfaces on dislocation mobility, the edge dislocation glide process in thin silicon films is modeled using an interatomic potential and first principles calculations. The influence of film thickness is determined, starting with the simulation of a silicene monolayer and then increasing the number of layers. The energy barrier for dislocation glide in silicene was calculated to be 1.5 eV, indicating a relatively high mobility of dislocation defects. In thin Si films a glide mechanism via consecutive bond rotations was identified, with kink nucleation being observed at the free surfaces of the film with subsequent migration. The influence of the free edge in finite size films is shown to be negligible in relation to glide for dislocations at distances from the free edge larger than three Burgers vectors. Molecular dynamics simulations reveal the possibility of more complex but lower energy barrier atomic reconstructions triggered at the free surfaces of the film near the dislocation core that may increase dislocation mobility at higher temperatures.

© 2020 Elsevier Ltd. All rights reserved.

## 1. Introduction

Silicon (Si) is one of the most technologically important chemical elements. It is still the work horse semiconducting material for modern electronic devices. While bulk (3D) silicon is massively produced (e.g. via the Czochralski process [1]) and used in industry, basic research on its single atom-thin 2D analog silicene is still in its infancy [2,3]. Between these extremes, the cutting edge technology FET (field effect transistors) centerpiece channel is a silicon fin of just a few nanometers thick, whose lattice quality is crucial to ensure low carrier (electrons or holes) scattering, high mobility, and ultimately best device performance. Can the ever present dislocations in such thin crystal be annealed and thus avoided? How can they move, and how would such thermally-activated motion depend on thickness-dimension, within a whole range from 2D-silicene to the 3D-wafer? This can be explored theoretically, and is a motivation and subject of this study.

Point-like and extended line defects are usually present in Si films after fabrication processes. The extended line defects known as dislocations play an important role in plastic response of a crystal. Dislocations are known to degrade the electronic properties of Si single crystal (SC); they perturb the crystal periodicity

and thus cause scattering of conduction electrons. Therefore, crystal defects are usually eliminated by annealing at high temperature, e.g. via furnace annealing [4] or rapid thermal annealing [5].

Due to Si abundance and its semiconducting properties, it can become a key building element for the next generation electronics. The thinnest Si film is monolayer silicene. Silicene – the silicon-based counterpart of graphene – is a two-dimensional monolayer material with a buckled honeycomb lattice that exhibits a range of promising electronic properties [6,7]. It was first investigated theoretically [2] and recently synthesized on different metallic substrates [3]. In spite of silicene's recent discovery, room temperature-operating silicene-based field-effect transistors have already been produced and tested [8]. At the same time, there are difficulties associated with the process of silicene fabrication, largely caused by its instability when exposed to air as well as high reactivity to oxygen. Therefore, other Si-based nanomaterials are considered. For example, bilayer silicene materials are claimed to be a better option in electronic applications, see e.g. study [9], in which such materials are synthesized and analyzed.

Numerous works were devoted to investigation of dislocation defects in bulk Si material with focus on their core structures and migration mechanism, including calculations of kink formation and migration energy barriers [10–13]. In order to understand the details of the annealing process and reveal the effect of finite thickness on dislocation migration process, in this work

\* Corresponding author.

E-mail address: [evgeniya.dontsova@enovate.ai](mailto:evgeniya.dontsova@enovate.ai) (E. Dontsova).

we investigate the glide process of an edge dislocation in thin Si films for different thicknesses starting from a silicene monolayer. This paper is structured as follows: first, the computational methods are described in the methodology section; next, results for silicene and then for thin Si films are presented, including energy barrier calculations and molecular dynamics simulations of the dislocation glide process; finally, the main findings are summarized.

## 2. Methodology

In the present work, calculations of atomic structures of Si films were performed using the molecular statics method implemented in LAMMPS [14], using the Stillinger–Weber (SW) interatomic potential developed for Si [15]. SW is an empirical potential that consists of two- and three-body terms that attempt to describe complex interatomic interactions. It was constructed to model solid and liquid forms of Si by fitting to the experimentally measured bulk properties. SW is one of the most used potentials for Si crystal because it provides a reasonably good description of its overall behavior. However, the SW potential provides a relatively poor description of low-buckled silicene material. For example, it predicts a buckling wavelength magnitude of 0.784 Å, almost two times higher than the 0.435 Å predicted by the more accurate first-principles calculations.

In order to capture an edge dislocation glide process in silicene (as well as 1.5- and 2-“silicene layers” thick Si films), we use a density functional theory (DFT) method based on the plane-wave basis set with a cutoff energy of 30 Ry (408 eV) in a local density approximation using Gaussian pseudopotentials [16], as implemented in the Quantum Espresso (QE) simulation package. For elastic constants calculations of silicene, 1.5- and 2-layers Si films, the Brillouin zone was sampled according to the Monkhorst–Pack [17] scheme with a  $16 \times 16 \times 1$  k-point mesh for unit cells composed of four, six, and eight Si atoms, respectively. To minimize the interactions between the neighboring cells the vacuum space between layers was set to at least 15 Å in the out-of-plane direction while maintaining in-plane periodicity. While for the isolated domain constructed to model the dislocation, only  $\Gamma$  point has been considered for the Brillouin zone sampling and the vacuum space between periodic images was set to at least 15 Å in all three directions to avoid spurious interactions. In addition, the free edges were hydrogenated in order to eliminate unpaired electrons.

We first examine the Si film stability and compare the SW results with representative DFT predictions of the energy of the optimized defect-free structure measured per atom and with respect to bulk Si SC in cubic diamond phase, as demonstrated in Fig. 1(a). The empirical potential and the DFT results show the same trend: the energy monotonically increases with decreasing film thickness; the highest value is associated with the least stable Si monolayer. Si in the bulk phase appears to be more stable than Si film of finite thickness, as expected.

To determine the minimum energy path (MEP) and corresponding energy barrier for edge dislocation glide process in Si films, including silicene, we employed the nudged elastic band (NEB) technique [18] as implemented in both simulation packages mentioned above. We used 21 images for SW potential calculations and 7 for DFT simulations.

### 2.1. Boundary conditions

A single dislocation introduces a displacement discontinuity across the glide plane which breaks down periodicity of the system and produces elastic fields that may persist over long distances depending on the boundary conditions. To overcome

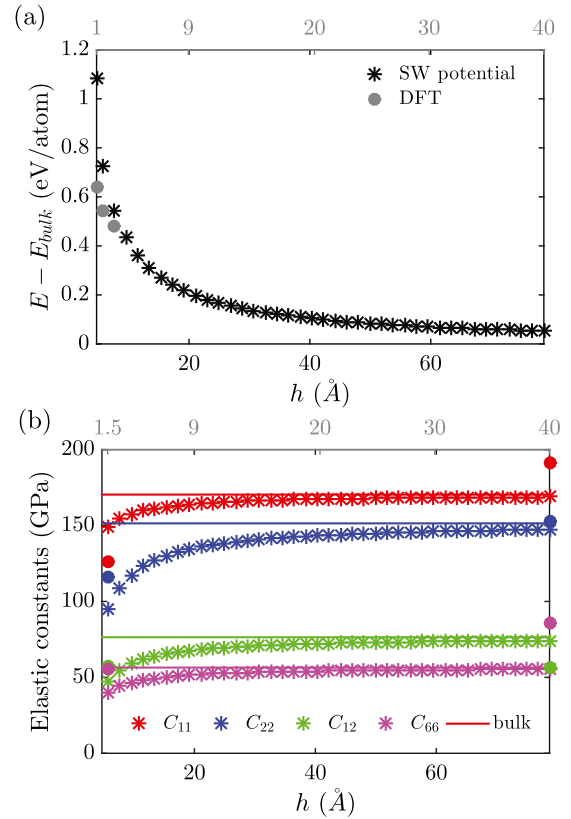


**Fig. 1.** (a) Energy per atom with respect to bulk diamond cubic Si SC and (b) elastic constants computed (see Appendix A) with the SW potential (asterisk symbols for finite thickness and solid lines for bulk Si SC) and a few DFT calculated values (filled circles) as functions of Si film thickness. Here bottom horizontal axis provides thickness  $h$  in Å while the top horizontal axis indicates the number of “silicene layers”. (For interpretation of the references to color in this figure legend, the reader is referred to the web version of this article.)

this issue different boundary conditions have been developed to model dislocation defects [21], such as the cluster approach, flexible boundary conditions [22], and periodic boundary conditions with dislocation dipoles. Here we use the cluster approach, an approximation for a single dislocation in an infinite medium, achieved by applying the corresponding linear elastic anisotropic material solution to an initially perfect SC simulation domain of finite size. The initial structure is relaxed to obtain the optimal dislocation core structure keeping the outermost atoms fixed to approximate the infinite medium.

The linear elastic solution for an edge dislocation in an anisotropic medium can be found in [20]. It requires appropriate elastic constants input for a chosen crystal orientation. The elastic constants calculated with the SW potential (and a few points with DFT method) for an anisotropic Si films, being oriented along  $[1\bar{1}0]$ ,  $[00\bar{1}]$ , and  $[110]$  crystallographic directions for  $x$ ,  $y$ , and  $z$ -axis, respectively, as functions of thickness  $h$ , that runs parallel to the  $z$ -axis, are shown in Fig. 1(b). The details of the procedure and approximations for calculating of the presented elastic constants for Si films are described in Appendix A. It can be seen from Fig. 1(b) that all displayed elastic constants decrease with decreasing thickness for the SW empirical potential, in agreement with DFT results also shown.

Fig. 2 demonstrates the procedure for inserting an edge dislocation of  $\mathbf{b} = \frac{1}{2}[110]$  Burgers vector, positioned at the origin of the coordinate system, into a Si film, here a 1.5-“silicene layers” thick film (also referred here as  $n_z = 1.5$ ), by applying the displacement associated with the linear elastic field given by

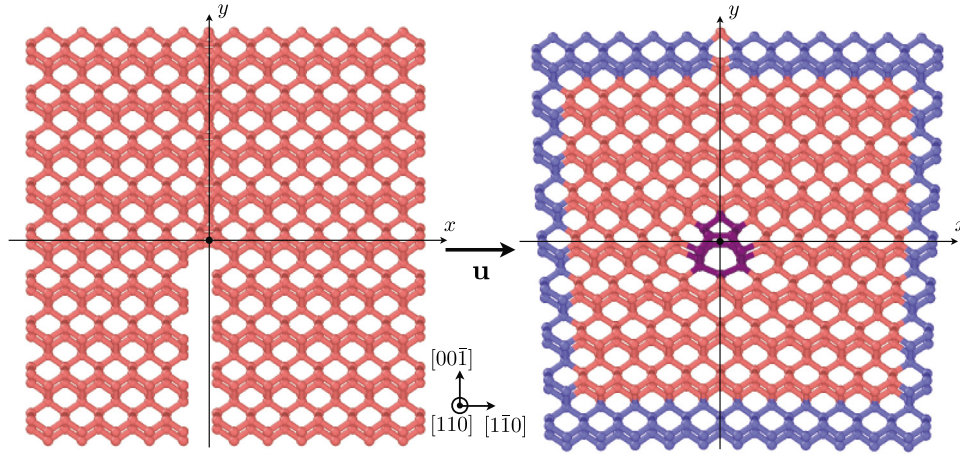


**Fig. 2.** Atomic representation (visualized with OVITO software developed in [19]) of (left) the initially “perfect” film structure with  $h = 5.8 \text{ \AA}$  or  $n_z = 1.5$  and (right) structure with an edge dislocation with  $\mathbf{b} = \frac{1}{2}[1\bar{1}0]$  obtained by displacing atoms of the “perfect” structure according to the linear elasticity solution in anisotropic material [20]. In the left structure atoms shown in salmon pink are allowed to relaxed while atoms colored in orchid blue remain fixed during energy minimization. (For interpretation of the references to color in this figure legend, the reader is referred to the web version of this article.)

Eq. (B.1) in Appendix B and using the computed elastic constants shown in Fig. 1(b). Since the discontinuous component of displacement field ( $u_x$ ) is symmetric with respect to the  $y$ -axis, an extra row of atoms should be deleted (inserted) below (above) the glide plane to have a complete discontinuity jump of minimal periodicity, i.e. having the total Burgers vector magnitude, above the glide plane to create a “perfect” film structure prior to dislocation insertion, see Fig. 2(left). Next, the dislocation is inserted by displacing this “perfect” structure, as shown in Fig. 2(right). Note that the latter structure is not yet relaxed, but the core structure composed of connected pentagon and heptagon rings is relatively well captured for an edge dislocation of glide type, i.e. with glide plane that runs along the closely spaced planes.

To reduce the effect of fixed boundary conditions on the energies of the initial and final structures (that differ by dislocation position of one complete glide step, and hence, produce an asymmetric MEP outcome) an appropriate shear strain in the  $xy$ -plane ( $\gamma$ , that reflects the work done by moving a dislocation by  $b/2$ ) is applied for both initial and final structures to have the same energy.

### 3. Results and discussion

#### 3.1. Silicene

We start with modeling of the glide of an edge dislocation in monolayer silicene using the NEB method with DFT calculations as described in Section 2. To introduce an edge dislocation in silicene (as for all calculations with thicker Si films) we use the isotropic linear elastic solution for an edge dislocation in an infinite medium. This avoids issues arising with the definition of thickness in the monolayer material. The isotropic solution requires knowledge of only Poisson’s ratio (see expressions for displacements in eqs. (3-45,46) in [20]), which we compute in a way similar to other elastic constants, as described in Appendix A. The initially relaxed silicene is stretched by  $\delta = 1\%$  along one direction and the optimal strain in the transverse direction (in-plane) is found by applying a set of deformations and fitting the strain energy data to a quadratic function. This allows us to calculate both in-plane Poisson’s ratios  $\nu_{xy} = -\varepsilon_{yy}/\delta$  and  $\nu_{yx} = -\varepsilon_{xx}/\delta$  which are 0.258 and 0.270, respectively. To use the elastic continuum model for inserting an edge dislocation in a monolayer silicene, we take the average value of the in-plane ratios, i.e.  $\nu = 0.264$ .

Moving on to dislocation glide, Fig. 3(a) shows the initial, saddle point, and final images for zero applied shear strain, i.e.  $\gamma = 0$ , calculated using the NEB method with corresponding MEP presented in Fig. 3(b). In order to reduce the effect of fixed boundary conditions that lead to different energies for the initial and final structures, a small shear strain is applied. We found that 3% shear strain leads to almost identical total energies for the initial and final structures, and hence more accurate measures of the energy barrier. Moreover, according to the data summarized in the table form in Fig. 3(c), the average value of the forward and backward energy barriers provides a good estimate for the barrier of a single edge dislocation to glide in an infinite medium of silicene despite the accumulated shear energy difference forced by the fixed boundary conditions.

#### 3.2. Silicon film

The Si film constructed for the considered crystal orientation can be symmetric and asymmetric with respect to the plane lying at the middle of the thickness while having the same structure of the free surfaces. Fig. 4 shows two cases when thickness has fractional  $n_z = 1.5$  and integer  $n_z = 2$  number of “silicene layers” that correspond to symmetric and asymmetric film surfaces. Moreover, the free surface structure affects the edge dislocation core structure: core atoms located at the top and bottom free surfaces have identical arrangements in case of symmetry, i.e.  $n_z = 1.5$ , as shown in Fig. 4(a), while arrangement differs for asymmetric free surfaces, i.e.  $n_z = 2$ , see Fig. 4(b).

Next, in order to reveal the effect of the dislocation core symmetry we perform the NEB calculation for one complete glide step of the  $\frac{1}{2}[1\bar{1}0]$  edge dislocation in both 1.5 and 2-layers Si films. As can be seen from Fig. 5(a, b) that include images labeled by the reaction coordinate (RC) values from the found MEP, the dislocation glides in a stepwise fashion by sequential bond rotations, in accordance with expectations. Note that NEB predicts this sequential bond rotation by itself for  $n_z \geq 2$  (for  $n_z = 1.5$  left unguided NEB predicts a higher energy path with simultaneous two bond rotation and 2.21 eV single energy barrier), if the initial and final structures that differ by one complete dislocation glide step are used as an input. The energy variation along the MEP presented in Fig. 5(c) demonstrates a noticeable difference for symmetric and asymmetric core geometries, yielding higher energy barrier for asymmetric case with rotated bond surrounded by larger number of neighboring atoms. More precisely, the table shown in Fig. 5(d) summarizes the calculated forward and

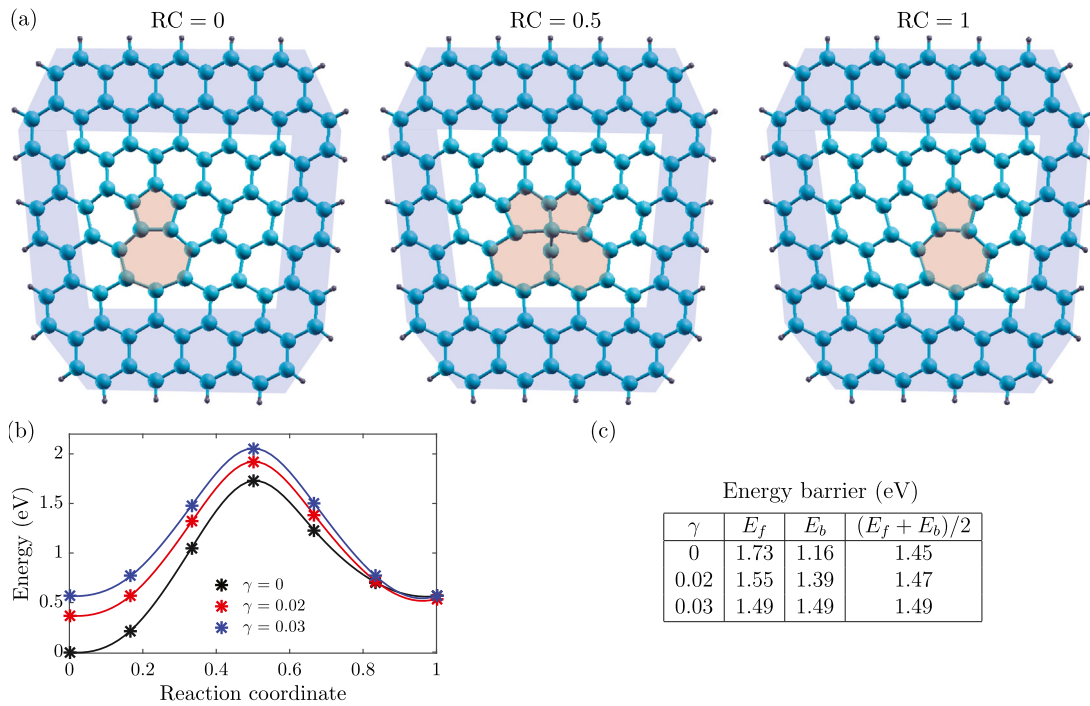


**Fig. 3.** (a) Atomic images of silicene containing an edge dislocation with hydrogenated free edges along MEP found using NEB method with DFT calculations. Here larger (smaller) blue (gray) circles represent Si (H) atoms. Atoms being fixed during the relaxation are shown under the hatched area. (b) Plot of the total energy as function of reaction coordinate along the MEP for different levels of applied shear strain  $\gamma$ . (c) Table of the corresponding forward  $E_f$  and backward  $E_b$  energy barriers as well as their averaged value for different shear strains. (For interpretation of the references to color in this figure legend, the reader is referred to the web version of this article.)

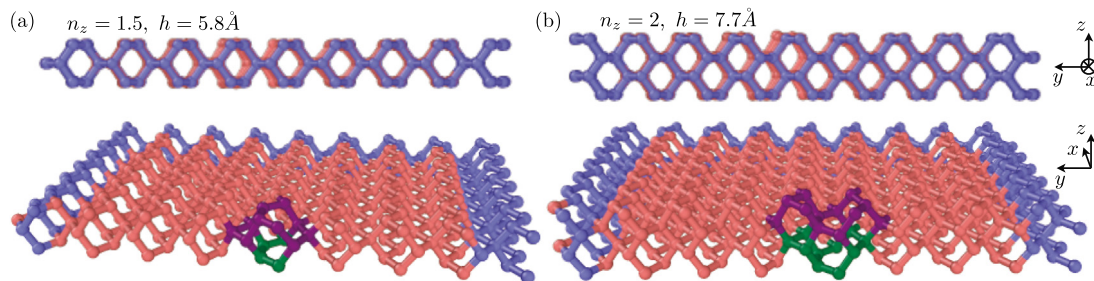


**Fig. 4.** (top) Atomic structure of Si films containing an edge dislocation of  $\mathbf{b} = \frac{1}{2}[1\bar{1}0]$  Burgers vector with (a)  $n_z = 1.5$  and (b)  $n_z = 2$  thicknesses in terms of “silicene layers”. (bottom) Atoms that compose the edge dislocation core in these Si films cuts are shown by purple and green colors for upper and lower layers along  $z$ -axis, displaying different core symmetries for fractional and integer  $n_z$ . (For interpretation of the references to color in this figure legend, the reader is referred to the web version of this article.)

backward energy barriers, namely  $E_f$  and  $E_b$ , for different bond rotations, that correspond to stepwise dislocation glide process (i.e. one bond rotation can be associated with a double-kink formation), along the dislocation line including rotation of single bond and in specific sequence for both  $n_z = 1.5$  and  $n_z = 2$  Si film thicknesses. For example, the symmetric core has a 1.26 eV energy barrier for a single bond rotation at both surfaces while asymmetric has 1.35 eV for the same surface and higher value of 1.72 eV for the other surface. This can be explained by more “bulk-like” atomic surroundings for the latter bond which leads to higher resistance for bond rotation.

To address the effect of thickness on the dislocation glide process we study 4.5-layers Si film having symmetric free surfaces. The side and top views of the edge dislocation core structure in 4.5-layers film is presented in Fig. 6(a), where the core atoms belonging to different layers (one layer has one pentagon–heptagon pair) are colored differently, while bonds that rotate during glide are all displayed in gray color. NEB with initial and final structures, where one complete dislocation glide step is overcome,

predicts a 32415 sequence for bond rotations with MEP shown by dotted line in Fig. 6(b). Namely, the middle bond labeled 3, see Fig. 6(a), rotates first, then bond 2 below, after that bond 4 above, bond 1 at the bottom and finally bond 5 at the top surface of the film. However, it is clearly not the most favorable path since bonds at the free surfaces have a lower energy barrier for rotation, as can be seen from the plot of nucleation barrier (black symbols) found for a single bond rotation versus bond position along  $z$ -axis in Fig. 6(c). Surface bonds within the dislocation core labeled by 1 and 5 have 1.36 eV energy barrier, next layers with bonds 2 and 4 have 1.99 eV, while 3rd bond has highest value of 2.03 eV. This result also shows that the influence of the free surface becomes insignificant at distances that are at least one layer away from it, as evident from the calculated energy barrier for bond rotation variation with distance to the free surface.

Next, we compare the MEP results presented in Fig. 6(b) for different bond rotation sequences, such as initial 32415 (predicted by NEB for the whole glide process), 15243 (the bonds with lower barriers are rotated first) and 12345 (glide starts from the

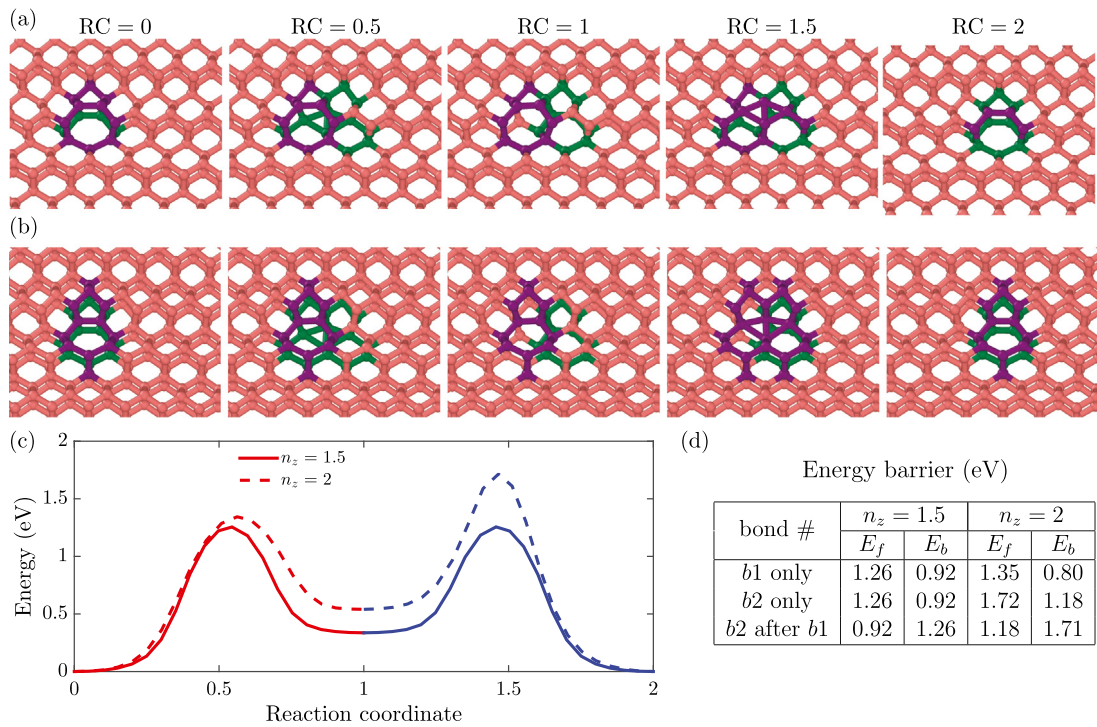


**Fig. 5.** NEB calculations with SW potential for one complete glide step of an edge dislocation in 1.5- and 2-layers Si films. Atomic representations of sequential images along the reaction path for dislocation core during glide for (a)  $n_z = 1.5$  and (b)  $n_z = 2$ . (c) MEP of sequential bond rotations for both films, which numerical values are summarized in table shown in (d). (For interpretation of the references to color in this figure legend, the reader is referred to the web version of this article.)

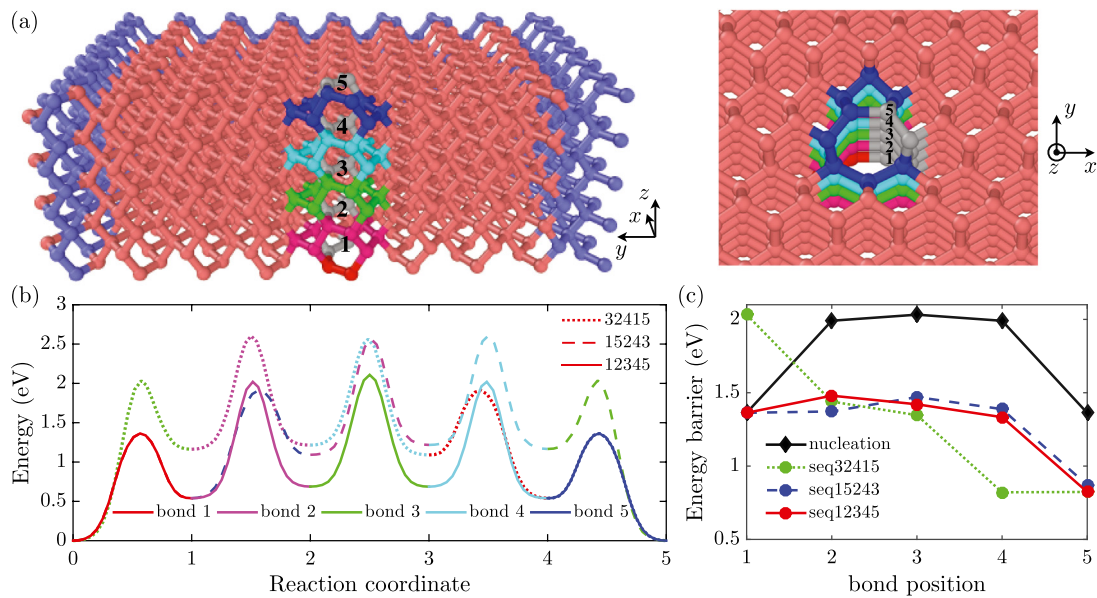


**Fig. 6.** Atomic structure of  $n_z = 4.5$  Si film (left) cut in the middle of the simulation domain along  $x$ -axis to display dislocation core, (right) top view on the core structure, where different colors correspond to different layers along  $z$ -axis, while bonds that undergo rotation during glide are shown in gray color and numbered according to  $z$  coordinate. NEB calculated (b) MEP for one complete glide step via different sequences of bond rotations and (c) corresponding energy barriers as functions of rotated bond position and sequence. (For interpretation of the references to color in this figure legend, the reader is referred to the web version of this article.)

surface and propagates till the opposite free surface) sequences obtained by sequential NEB calculations with one bond rotated at a time. The corresponding energy barrier for each bond rotation in these sequences as function of bond number or position is also in shown Fig. 6(c). Clearly, the 12345 sequence provides the lowest energy path among the considered sequences with slow variation of the energy barrier, except for the last step, along the path and

with lowest energies for the intermediate structures (i.e. when the one bond rotation is complete). In turn, the 32415 sequence has a noticeably higher initial barrier, but also displays a lowest barrier for the next to last bond rotation in comparison with other sequences. Therefore, 12345 is considered as the MEP for the one complete edge dislocation glide step in 4.5-layers Si film. We conclude that such a sequential glide propagation mechanism

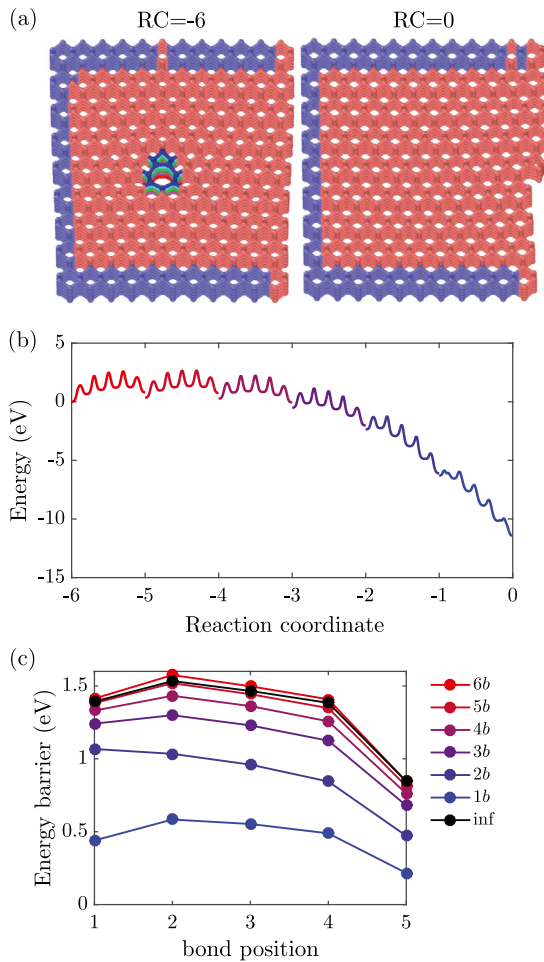


**Fig. 7.** Atomic structures of 4.5-layers Si film with an edge dislocation (a)  $6b$  and (b)  $0b$  away from the free edge. Here atoms shown in salmon pink are allowed to relaxed while atoms colored in orchid blue remain fixed during energy minimization. The NEB calculated (c) MEP for the edge dislocation glide toward the free edge initially  $6b$  away via 12345 sequence of bond rotations and (d) corresponding energy barrier for each bond rotation. (For interpretation of the references to color in this figure legend, the reader is referred to the web version of this article.)

should apply for other thicknesses in Si films. As a result, all further calculations are performed for this sequence (12345 in case of 4.5-layers film).

Another interesting aspect to investigate is the influence of finite film size on the dislocation glide process. In other words, to what extent does the barrier to glide (along  $x$ -direction) change when the dislocation approaches the free edge (equivalently, free surface in the  $yz$ -plane)? In case of the presence of a free edge the previously applied boundary conditions should be modified. Using the concept of images, this is done by simply adding the displacement field of an edge dislocation with Burgers vector of opposite sign at a distance equal to the distance between the original dislocation and the free edge, but keeping the free edge atoms unfixed, as shown in Fig. 7(a). The complete solution for an edge dislocation in the vicinity of a free surface however should also include a correction to the solution that eliminates the spurious traction components along the free surface [20]. But since this correction does not produce any force on the dislocation [20] and in our simulations the free edge atoms are not kept fixed, it is neglected.

The NEB predicted MEP for an edge dislocation  $6b$  away from the free edge (also labeled as  $RC = -6$ ) to glide all the way to

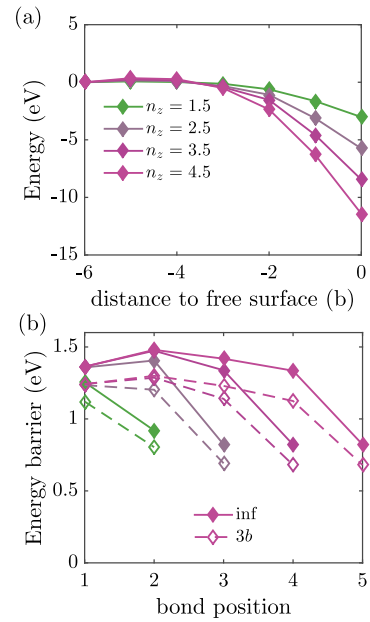


**Fig. 8.** (a) Total energy with respect to the value for the initial structure with dislocation located  $6b$  away from the free edge for Si film with different thicknesses. (b) Energy barrier for each sequential bond rotation for different film thicknesses with an edge dislocation in an infinite medium (filled symbols and solid lines) and  $3b$  distance away from the free edge (empty symbols and dashed lines). (For interpretation of the references to color in this figure legend, the reader is referred to the web version of this article.)

the free edge ( $RC = 0$ ) is shown in Fig. 7(b), where the initial and final structures for the whole glide process are displayed in Fig. 7(a), respectively. Note that this path was calculated in sequential manner, i.e. with the 12345 sequence of bond rotations for  $n_z = 4.5$  Si film for each complete glide step of Burgers vector in magnitude. The corresponding variation in energy barrier for each glide step labeled by “ $nb$ ”, where  $n$  runs from 6 to 0, is also included in Fig. 7(c) (here “inf” refers to the case without the free edge, i.e. for in-plane periodic film). Since the free edge boundary conditions depend on the dislocation position that changes during glide process, while fixed boundary conditions are desired in NEB calculations, some assumptions are needed. Here each complete glide step is performed under different boundary conditions that reflect the initial dislocation position. That is why a mismatch in energy can be observed in Fig. 7(b) when one glide step along the entire dislocation line is complete. Although we observe the discontinuity in MEP due to the fixed boundary conditions required by NEB set up, as can be seen in Fig. 7(b), that may lead to slight overestimation of the energy barrier.

According to Fig. 7(c), which shows the energy barriers versus rotated bond positions for different proximity of dislocation to the free edge, a noticeable effect of the free edge presence on dislocation glide process can be observed only at distances of  $3b$  and less. To be more specific, the initial bond rotation barrier (i.e. for bond position = 1) reduces from 1.38 eV for  $5b$  to 1.33 for  $4b$ , 1.24 for  $3b$ , 1.07 for  $2b$ , and finally 0.44 eV for  $1b$ .

In regard to the influence of thickness, the effect of the free edge on dislocation glide should be more pronounced in thicker films due to longer dislocation line and hence larger attractive force to the free edge. In agreement with expectations, Fig. 8(a) demonstrates the higher reduction in the total energy for thicker films when the distance between dislocation and free edge decreases. The comparison for the energy barrier versus bond position, where bonds are rotated in a sequential manner starting from the bottom film surface till the top one, for one complete

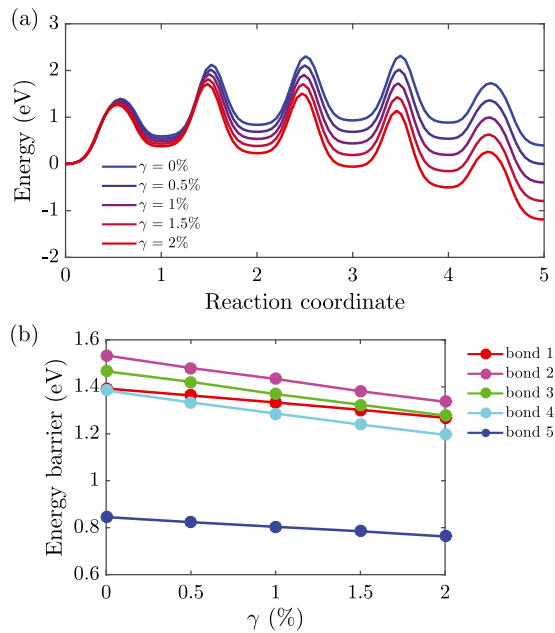


**Fig. 9.** NEB calculated (a) MEP for one complete glide step of an edge dislocation for 12345 sequence of bond rotations (see Fig. 6(a) for bonds numbering) under different shear deformations and (b) energy barriers for each rotated bond in the considered sequence as functions of applied shear strains for 4.5-layers Si film. (For interpretation of the references to color in this figure legend, the reader is referred to the web version of this article.)

dislocation glide step in an infinite medium and  $3b$  away from the free edge is also shown in Fig. 8(b) for different film thicknesses. Small variation of the barrier for initial and final bonds (i.e. bonds at the free surfaces of a film) and higher but rather close values for the “inner” bonds to rotate can be observed from this plot for a range of thicknesses, confirming a very local free edge effect on the barrier for an individual bond to undergo glide. In addition, the presence of the free edge (here  $3b$  from the dislocation core) the energy barrier curves for films with different thicknesses are simply shifted by approximately the same magnitude ( $\approx 0.2$  eV) reflecting that the attractive force per dislocation line due to the free edge is of similar magnitude, see Fig. 8(b).

Moving to the effect of an applied shear strain on the dislocation glide process, Fig. 9(a) shows the MEP for sequential bond rotations (starting from the bottom free surface, i.e. 12345 sequence of bonds) of an edge dislocation in 4.5-layers Si film under different shear strain values denoted by  $\gamma$ , whereas Fig. 9(b) demonstrates that the energy barrier for each bond decreases linearly with shear strain having similar slopes for internal bonds 2,3,4 and outermost bonds 1,5. Different slopes for “outer” and “inner” bonds, or equivalently, dislocation segments, reflect increase in resistance of kink to be formed at the “inner” position along the dislocation line in comparison with location near the top/bottom surface.

### 3.3. Molecular dynamics simulation of dislocation glide in Si film

In order to identify the glide mechanism, we performed molecular dynamics (MD) calculations using the SW potential under the NVT ensemble at  $T = 610$  K for 4.5-layers Si film with an edge dislocation subjected to 4% shear strain in the  $xy$ -plane. Similar boundary conditions are used for dynamic calculations, i.e. the outermost atoms along the simulation domain perimeter are kept fixed, while the rest are allowed to move.

The edge dislocation glide is observed in the described above MD simulation, as shown in Fig. 10 for different domain slices.

Specifically, initial atomic reconstruction occurs near the dislocation core at free surfaces of the film. Subsequently, according to results demonstrated in Fig. 10(a), bond rotation is observed in the next to the free surface layer (i.e. bond 2 from the previous notation for 4.5-layers Si film) when simulation time of 7.5 ns is achieved. Next, at about 29 ns more complicated atomic rearrangement happens near the dislocation core that involves both 3rd and 4th layers along  $z$ -axis after which the whole dislocation line shifts by one complete glide step, see Fig. 10(b).

According to the careful study that compares static and dynamic atomic-scale simulations of kink-pair nucleation on dislocations, or equivalently, dislocation glide process [23], the kink nucleation at the dislocation line is well captured by the simple thermally activated law. Namely, the average time  $t$  required for the formation of one stable kink pair can be determined as  $t = \frac{1}{\nu_D} \exp(\frac{H}{k_B T})$ , where  $\nu_D \simeq 10^{13}$  Hz is the silicon Debye frequency,  $k_B T$  is the thermal energy,  $H$  is the activation enthalpy. Based on our results of energy barrier calculations, the time estimate for 2nd bond to rotate (the energy barrier is  $H = 1.16$  eV at 4% shear strain) should be  $\simeq 0.4$  ms which is 4 orders of magnitude slower than 7.5 ns observed in MD simulations. Consequently, the atomic reconstructions that happen near the dislocation core at the top/bottom surfaces may lead to substantial energy barrier reduction and facilitate much faster kink migration, in our case achieved via simple bond rotation. Besides, more complex atomic rearrangement triggered at the free surfaces near the dislocation core as well may lead to the barrier reduction and glide of larger segments of the dislocation line, as indicate our MD simulations, where simultaneous propagation of 3rd and 4th bonds is observed at 29 ns of run time.

## 4. Summary

First-principles and interatomic potential calculations have been performed to investigate the edge dislocation glide mechanism in monolayer silicene and thicker Si films, respectively. The computed energy barrier of 1.5 eV for dislocation glide in silicene appears to be significantly lower than graphene’s 7 eV [24], indicating higher dislocation mobility in silicene. For thin Si films we found that the glide process of an edge dislocation, having pentagon–heptagon core structure at each layer, is achieved via consecutive bond rotations starting from the free top (bottom) surface of the film. The interactions between dislocation and free edge in finite-size Si films become important or noticeably reduce the barrier to glide only for the distance of 3 or less in terms of Burgers vector magnitude, meaning that this effect can be neglected for dislocation travel time estimations. Moreover, MD simulations show that glide mechanisms via more complex bond rearrangements are possible and may increase the dislocation mobility at higher temperatures. To conclude, the presence of top and bottom free surfaces in Si films provides a starting point for dislocation migration by facilitating initial kink formation that promotes further propagation.

### Declaration of competing interest

The authors declare that they have no known competing financial interests or personal relationships that could have appeared to influence the work reported in this paper.

### Appendix A. Elastic constants

A cubic diamond Si SC possesses a cubic crystal symmetry which implies that it has only three independent elastic constants, namely  $C_{11}^{(0)}$ ,  $C_{12}^{(0)}$ ,  $C_{44}^{(0)}$ . In case when the coordinate system is oriented along crystals’ highest symmetry directions, i.e.  $\langle 100 \rangle$ ,

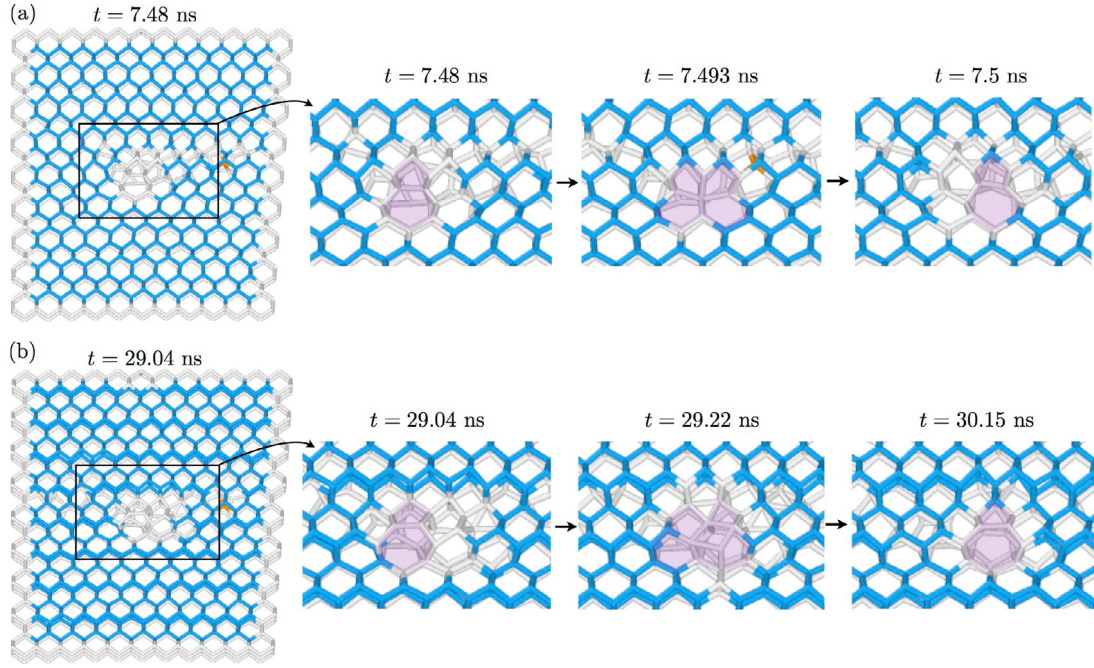


**Fig. 10.** MD simulation snapshots of 4.5-layers Si film with an edge dislocation at  $T = 610$  K under applied shear strain  $\gamma = 4\%$  sliced along  $z$ -direction at (a) 2nd and (b) 4th layers. Here blue color corresponds to bonds between atoms having cubic diamond environment, while gray represent other atomic coordination reflecting dislocation core and free surface atoms. The whole simulation domain (left), as well as zoomed images near the dislocation core are included. (For interpretation of the references to color in this figure legend, the reader is referred to the web version of this article.)

the elastic stiffness tensor writes in matrix form using the Voigt notation as

$$\mathbf{C}^{(0)} = \begin{bmatrix} C_{11}^{(0)} & C_{12}^{(0)} & C_{12}^{(0)} & 0 & 0 & 0 \\ C_{12}^{(0)} & C_{11}^{(0)} & C_{12}^{(0)} & 0 & 0 & 0 \\ C_{12}^{(0)} & C_{12}^{(0)} & C_{11}^{(0)} & 0 & 0 & 0 \\ 0 & 0 & 0 & C_{44}^{(0)} & 0 & 0 \\ 0 & 0 & 0 & 0 & C_{44}^{(0)} & 0 \\ 0 & 0 & 0 & 0 & 0 & C_{44}^{(0)} \end{bmatrix}, \quad (\text{A.1})$$

If the coordinate system is arbitrary rotated with respect to crystals' highest symmetry directions, the elastic stiffness tensor  $\mathbf{C}$ , that relates stress and strain tensors as  $\boldsymbol{\sigma} = \mathbf{C}\boldsymbol{\varepsilon}$ , can be obtained by applying the proper orthogonal transformation on the original fourth-rank  $\mathbf{C}^{(0)}$  tensor, see eq. (2-43) in [20].

To compute the three independent elastic constants of bulk Si SC, three different displacement boundary conditions are imposed and elastic constants are extracted from the quadratic function fit of the calculated strain energies as functions of applied strain. Specifically, the applied strain and corresponding strain energy in each case are (1)  $\varepsilon_{xx} = \delta$ ,  $E = C_{11}^{(0)}\delta^2/2$ ; (2)  $\varepsilon_{xx} = \delta$  and  $\varepsilon_{yy} = \delta$ ,  $E = (C_{11}^{(0)} + C_{12}^{(0)})\delta^2$ ; (3)  $2\varepsilon_{xy} = \delta$ ,  $E = C_{44}^{(0)}\delta^2/2$ ; where  $\delta \in [-0.001, 0.001]$ . For instance, SW potential predicts 151.4, 76.4, and 56.4, while DFT method gives 153.2, 56.7 and 86.2 values for  $C_{11}^{(0)}$ ,  $C_{12}^{(0)}$ ,  $C_{44}^{(0)}$  elastic constants in GPa, respectively.

A Si film of finite thickness (along  $z$ -axis) is considered under plane stress condition and necessary in-plane ( $xy$ -plane) elastic constants, i.e.  $C_{11}$ ,  $C_{22}$ ,  $C_{12}$ , and  $C_{66}$ , are found in similar manner by fitting strain energies versus applied strains, but using the elastic constants which dictate the out-of-plane deformations for properly oriented bulk Si SC. In details, the applied strain and corresponding strain energy are (1)  $\varepsilon_{xx} = \delta$  (since  $\sigma_{zz} = 0$ , there is also non-zero  $\varepsilon_{zz} = -\frac{C_{13}^b}{C_{33}^b}\delta$  that was not imposed, but comes from relaxation of the traction-free surfaces),  $E = (C_{11} - C_{13}^b \frac{C_{13}^b}{C_{33}^b})\delta^2/2$ ;

(2)  $\varepsilon_{yy} = \delta$  ( $\varepsilon_{zz} = -\frac{C_{23}^b}{C_{33}^b}\delta$ ),  $E = (C_{22} - C_{23}^b \frac{C_{23}^b}{C_{33}^b})\delta^2/2$ ; (3)  $\varepsilon_{xx} = \delta$ ,  $\varepsilon_{yy} = -\delta$  ( $\varepsilon_{zz} = \frac{(C_{23}^b - C_{13}^b)}{C_{33}^b}\delta$ ),  $E = ((C_{11} + C_{22}) - 2C_{12} - \frac{(C_{13}^b - C_{23}^b)^2}{C_{33}^b})\delta^2/2$ ; (4)  $2\varepsilon_{xy} = \delta$ ,  $E = C_{66}\delta^2/2$ . Here  $C$  constants labeled with "b" superscript are for bulk Si SC oriented along  $[1\bar{1}0]$ ,  $[00\bar{1}]$ , and  $[110]$  directions for  $x$ ,  $y$ , and  $z$ -axis, while  $\delta \in [-0.001, 0.001]$ . To calculate the volume needed for the strain energy evaluation the film thickness is approximated by  $h = n_z\sqrt{2}a_0$ , where  $n_z$  is the number of layers in terms of the minimal periodicity along  $[110]$  directions ( $n_z$  can also be referred to the number of "silicene layers" for the considered geometry),  $a_0$  is the lattice constant of bulk Si SC that is 5.43 Å for SW potential and 5.46 Å from DFT calculations.

## Appendix B. Linear elastic solution for an edge dislocation in anisotropic medium

According to [20] (see eq. (13-116)), linear elastic solution for displacement  $\mathbf{u} = (u_x, u_y, u_z)$  due to the pure edge dislocation with Burgers vector  $\mathbf{b} = (b_x, 0, 0)$  and dislocation line along  $\xi = (0, 0, -1)$  in an infinite anisotropic medium writes in Cartesian coordinates (denoted by  $x$ ,  $y$ , and  $z$ ) as:

$$\begin{aligned} u_x &= \frac{b_x}{4\pi} \left[ \tan^{-1} \frac{2xy\lambda \sin \phi}{x^2 - \lambda^2 y^2} + \frac{C_{11}^2 - C_{12}^2}{2C_{11}C_{66} \sin 2\phi} \ln \frac{q}{t} \right], \\ u_y &= \frac{\lambda b_x}{4\pi C_{11} \sin 2\phi} \left[ (C_{11} - C_{12}) \cos \phi \ln qt \right. \\ &\quad \left. - (C_{11} + C_{12}) \sin \phi \tan^{-1} \frac{\lambda^2 y^2 \sin 2\phi}{x^2 - \lambda^2 y^2 \cos 2\phi} \right], \\ u_z &= 0, \end{aligned} \quad (\text{B.1})$$

where additionally introduced quantities are  $\lambda = (C_{11}/C_{22})^{1/4}$ ,  $\phi = \frac{1}{2} \cos^{-1} \frac{C_{12}^2 + 2C_{12}C_{66} - C_{11}^2}{2C_{11}C_{66}}$ ,  $q = x^2 + 2xy\lambda \cos \phi + y^2\lambda^2$ ,  $t = x^2 - 2xy\lambda \cos \phi + y^2\lambda^2$ . Here  $C_{ij}$  refer to elastic constants of a material.

## References

- [1] Fumio Shimura, *Single-Crystal Silicon: Growth and Properties*, Springer International Publishing, Cham, 2017, pp. 293–307.
- [2] Gian G. Guzman-Verri, L.C. Lew Yan Voon, Electronic structure of silicon-based nanostructures, *Phys. Rev. B* 76 (2007) 075131.
- [3] Patrick Vogt, Paola De Padova, Claudio Quaresima, Jose Avila, Emmanouil Frantzeskakis, Maria Carmen Asensio, Andrea Resta, Bénédicte Ealet, Guy Le Lay, Silicene: Compelling experimental evidence for graphenelike two-dimensional silicon, *Phys. Rev. Lett.* 108 (2012) 155501.
- [4] C. Christofides, Annealing kinetics of defects of ion-implanted and furnace-annealed silicon layers: thermodynamic approach, *Semicond. Sci. Technol.* 7 (11) (1992) 1283.
- [5] B. Rau, T. Weber, B. Gorka, P. Dogan, F. Fenske, K.Y. Lee, S. Gall, B. Rech, Development of a rapid thermal annealing process for polycrystalline silicon thin-film solar cells on glass, *Mater. Sci. Eng. B* 159 (2009) 329–332.
- [6] Abdelkader Kara, Hanna Enriquez, Ari P. Seitsonen, L.C. Lew Yan Voon, Sébastien Vizzini, Bernard Aufray, Hamid Oughaddou, A review on silicene – new candidate for electronics, *Surf. Sci. Rep.* 67 (1) (2012) 1–18.
- [7] M. Houssa, A. Dimoulas, A. Molle, Silicene: a review of recent experimental and theoretical investigations, *J. Phys.: Condens. Matter* 27 (25) (2015) 253002.
- [8] Li Tao, Eugenio Cinquanta, Daniele Chiappe, Carlo Grazianetti, Marco Fanciulli, Madan Dubey, Alessandro Molle, Deji Akinwande, Silicene field-effect transistors operating at room temperature, *Nat. Nanotechnol.* 10 (3) (2015) 227–231.
- [9] Ritsuko Yaokawa, Tetsu Ohsuna, Tetsuya Morishita, Yuichiro Hayasaka, Michelle J.S. Spencer, Hideyuki Nakano, Monolayer-to-bilayer transformation of silicenes and their structural analysis, *Nature Commun.* 7 (10657) (2016).
- [10] S. Öberg, P.K. Sitch, R. Jones, M.I. Heggie, First-principles calculations of the energy barrier to dislocation motion in si and gaas, *Phys. Rev. B* 51 (1995) 13138–13145.
- [11] V.V. Bulatov, J.F. Justo, W. Cai, S. Yip, A.S. Argon, T. Lenosky, M. de Koning, T. Diaz de la Rubia, Parameter-free modelling of dislocation motion: The case of silicon, *Phil. Mag. A* 81 (5) (2001) 1257–1281.
- [12] L. Pizzagalli, A. Pedersen, A. Arnaldsson, H. Jónsson, P. Beauchamp, Theoretical study of kinks on screw dislocation in silicon, *Phys. Rev. B* 77 (2008) 064106.
- [13] Martin Kittler, Manfred Reiche, Structure and properties of dislocations in silicon, in: Sukumar Basu (Ed.), *Crystalline Silicon - Properties and Uses*, InTech, Rijeka, 2011 (Chapter 04).
- [14] Steve Plimpton, Fast parallel algorithms for short-range molecular dynamics, *J. Comput. Phys.* 117 (1) (1995) 1–19.
- [15] Frank H. Stillinger, Thomas A. Weber, Computer simulation of local order in condensed phases of silicon, *Phys. Rev. B* 31 (1985) 5262–5271.
- [16] C. Hartwigsen, S. Goedecker, J. Hutter, Relativistic separable dual-space gaussian pseudopotentials from h to rn, *Phys. Rev. B* 58 (1998) 3641–3662.
- [17] Hendrik J. Monkhorst, James D. Pack, Special points for brillouin-zone integrations, *Phys. Rev. B* 13 (1976) 5188–5192.
- [18] Graeme Henkelman, Blas P. Uberuaga, Hannes Jónsson, A climbing image nudged elastic band method for finding saddle points and minimum energy paths, *J. Chem. Phys.* 113 (22) (2000) 9901–9904.
- [19] Alexander Stukowski, Visualization and analysis of atomistic simulation data with ovito—the open visualization tool, *Model. Simul. Mater. Sci. Eng.* 18 (1) (2010) 015012.
- [20] J.P. Hirth, J. Lothe, *Theory of Dislocations*, in: *McGraw-Hill Series in Electrical Engineering: Electronics and Electronic Circuits*, McGraw-Hill, 1967.
- [21] D. Rodney, L. Ventelon, E. Clouet, L. Pizzagalli, F. Willaime, Ab initio modeling of dislocation core properties in metals and semiconductors, *Acta Mater.* 124 (2017) 633–659.
- [22] C. Woodward, First-principles simulations of dislocation cores, *Mater. Sci. Eng. A* 400–401 (2005) 59–67.
- [23] David Rodney, Activation enthalpy for kink-pair nucleation on dislocations: Comparison between static and dynamic atomic-scale simulations, *Phys. Rev. B* 76 (2007) 144108.
- [24] Chungheng Gong, Alex W. Robertson, Kuang He, Gun-Do Lee, Euijoon Yoon, Christopher S. Allen, Angus I. Kirkland, Jamie H. Warner, Thermally induced dynamics of dislocations in graphene at atomic resolution, *ACS Nano* 9 (10) (2015) 10066–10075.